Synthesis of lipophilic core-shell Fe3O4@SiO2@Au nanoparticles and polymeric entrapment into nano-micelle. A novel nanosystem for in vivo active targeting and magnetic resonance/ photoacoustic dual-imaging

Synthesis of lipophilic core-shell Fe_3O_4@SiO_2@Au nanoparticles and polymeric entrapment into nano-micelles. A novel nanosystem for *in vivo* active targeting and magnetic resonance and photoacoustic dual-imaging.

I. Monaco, [†] F. Arena, [‡] S. Biffi, [§] E. Locatelli, [†] B. Bortot, [§] F. La Cava [+], G. Marini, [‡] G. M. Severini, [§] E. Terreno [‡], M. Comes Franchini [†,*]

[†] *Department of Industrial Chemistry "Toso Montanari".* University of Bologna. Viale del Risorgimento 4, Bologna, 40136 Italy

[‡] *Molecular & Preclinical Imaging Centers, Department of Molecular Biotechnology and Healthy Sciences, University of Torino, Via Nizza 52, Torino, 10126, Italy.*

[§] *Institute for Maternal and Child Health- IRCCS "Burlo Garofalo", Via dell'Istria 65/1, 34137, Trieste, Italy.*

Abstract

In this work, iron/silica/gold core-shell nanoparticles (Fe_3O_4@SiO_2@Au NPs) characterized by magnetic and optical properties have been synthetized to obtain a promising theranostic platform. In order to improve their biocompatibility, the obtained multilayer nanoparticles have been entrapped in polymeric micelles (PMs), decorated with folic acid moieties and tested in vivo for Photoacustic (PA) and MRI detection of ovarian cancer.

Introduction

The increasing availability of nanomaterials with highly controlled magnetic and optical properties has created a great interest in the use of core-shell NPs in biological systems for diagnostic and therapeutic applications,[1] giving rise to the emerging concept of theranostics.[2] Magnetic NPs, especially based on Fe_3O_4 (magnetite) and Fe_2O_3 (maghemite), have attracted interest due to their superparamagnetism and good bio-tolerability that justify the high number of literature reports on the synthesis of magnetic core/shell nanoparticles in which the core is Fe_3O_4 and the shell consists of a metal or metal-oxide with peculiar optical properties.

Recently, much effort has been devoted to the synthesis and characterization of silica-coated iron-oxide NPs,[3] since the magnetic NPs are easily coated with amorphous silica via the sol–gel process.[4] Moreover, they can further react with gold NPs, thus creating a multilayer iron oxide/silica/gold nano-shells. Compared to the iron-oxide or iron oxide/silica core-shell NPs, the addition of gold layer extends the theranostic potential of the system due to the peculiar optical properties of this metal. Moreover, due to the high dielectric constant of silica, the three-layered Fe_3O_4/SiO_2/Au nanocomposite ensures a stronger light-absorption than the two-layered iron oxide/gold nanoshell. In spite of that, very few reports have appeared in the literature on these systems.

Kim *et al*. reported the synthesis of magnetic gold nanoshell as one of the first multifunctional nanomedical platforms characterized by magnetic and optical properties.[5] However, that system was not a core-shell type, because Fe_3O_4 and gold seed nanoparticles were assembled on amino-modified silica spheres. Li and Melancon coated commercially available iron-oxide NPs first with amorphous silica via the sol-gel process and then with gold nanocrystal seeds.[6,7] The obtained magnetic-Au nanoshells showed high r_2 and r_2/r_1 values and a strong NIR absorbance that make them suitable for MRI-guided photo-thermal therapy mediated by the application of external magnetic field.

However, the mere use of MRI modality for cancer early detection still has some limitations due to low sensitivity and specificity that can be partially overcome through the combination with other, possibly complementary, diagnostic techniques.[89]

Photoacoustic Imaging (PAI) represents an emerging diagnostic method with non-invasive and non-ionizing properties with ease applicability in clinical setup.[10] The combination of MRI and PAI could offer a way to overcome the depth and resolution limits of PAI and the relatively poor sensitivity in contrast agent detection of MRI.[11]

A similar approach was exploited in the recent work of Zhou *et al*., where multifunctional superparamagnetic iron oxide-containing gold nanoshell (SPIO@AuNS) nanoparticles have been used for guiding and monitoring by PA and MR dual imaging the photothermal ablation therapeutic effects in tumor bearing mice.[12]

It is noteworthy that surface functionalization is a key step to design hybrid organic-inorganic nanosystems, none of the published reports followed this approach, and only naked core-shell NPs were investigated so far. On the other hand, functional groups on the outer shell allowing for targetable nanocarriers containing core-shell NPs would be highly desirable because targeted nanostructures hold a lot of promises in biomedical applications.

In this work, we synthesized a multi-layered nanosystem constituted by a magnetic core of Fe_3O_4 NPs coated with an inner silica layer and outer gold shell. The so-obtained Fe_3O_4@SiO_2@Au NPs have been coated with an organic ligand by exchange ligand reaction to make them lipophilic and suitable for entrapment into biocompatible polymeric micelles (PMs). Then, folic acid (FA) has been conjugated on the PMs surface to obtain a water-soluble nanocarrier for targeting folate receptors (FR), which are overexpressed in many solid tumours, including ovarian cancer (Figure 1).[13] Finally, the potential of the developed system as bimodal MRI/PAI agent has been assessed *in vitro* and *in vivo* on a mouse model of ovarian cancer.

Results and discussion

Synthesis of Fe_3O_4@SiO_2@Au@PMs

The synthesis of the multi-layered nanosystem was accomplished by combining several procedures reported in literature. Iron oxide nanoparticles were synthetized with thermal decomposition method.[14] Silica shell was formed following sol-gel and Stober method:[15] by using the *oil-in-water* technique, a microemulsion with the surfactant agent CTAB was obtained, and silica shell thickness was controlled by adjusting the MTEOS/Fe_3O_4 NPs concentration. APTMS was added to produce positively charged amino groups onto silica surface: this allowed for electrostatically coating of the Fe_3O_4@SiO_2 core-shell system with the gold seeds obtained by Duff and Baiker's method,[16] which indeed present a negatively charged surface (Figure 1). The formation of an entire shell of gold performed by a shell growth reaction, where gold is mildly reduced, led to the multi-layered Fe_3O_4@SiO_2@Au NPs (see the experimental procedures in the Supporting Information for details). The obtained particles were fully characterized by Dynamic Light Scattering (DLS) and showed a hydrodynamic diameter of 222 nm, with a PDI of 0.251 and a ζ-potential of -32.2 mV (Figure S1). While, TEM images indicated that particles had a diameter in the range of 100 - 110 nm with a spherical shape and an external thickness silica shell of 20 nm (Figure S2). STEM and EDX mapping analysis confirmed the presence of the three different shells with iron in the core, silica in the middle and gold onto the surface (Figure S3). Atomic absorption analysis revealed an iron and gold concentration of 4.1 mM and 12.3 mM, respectively.

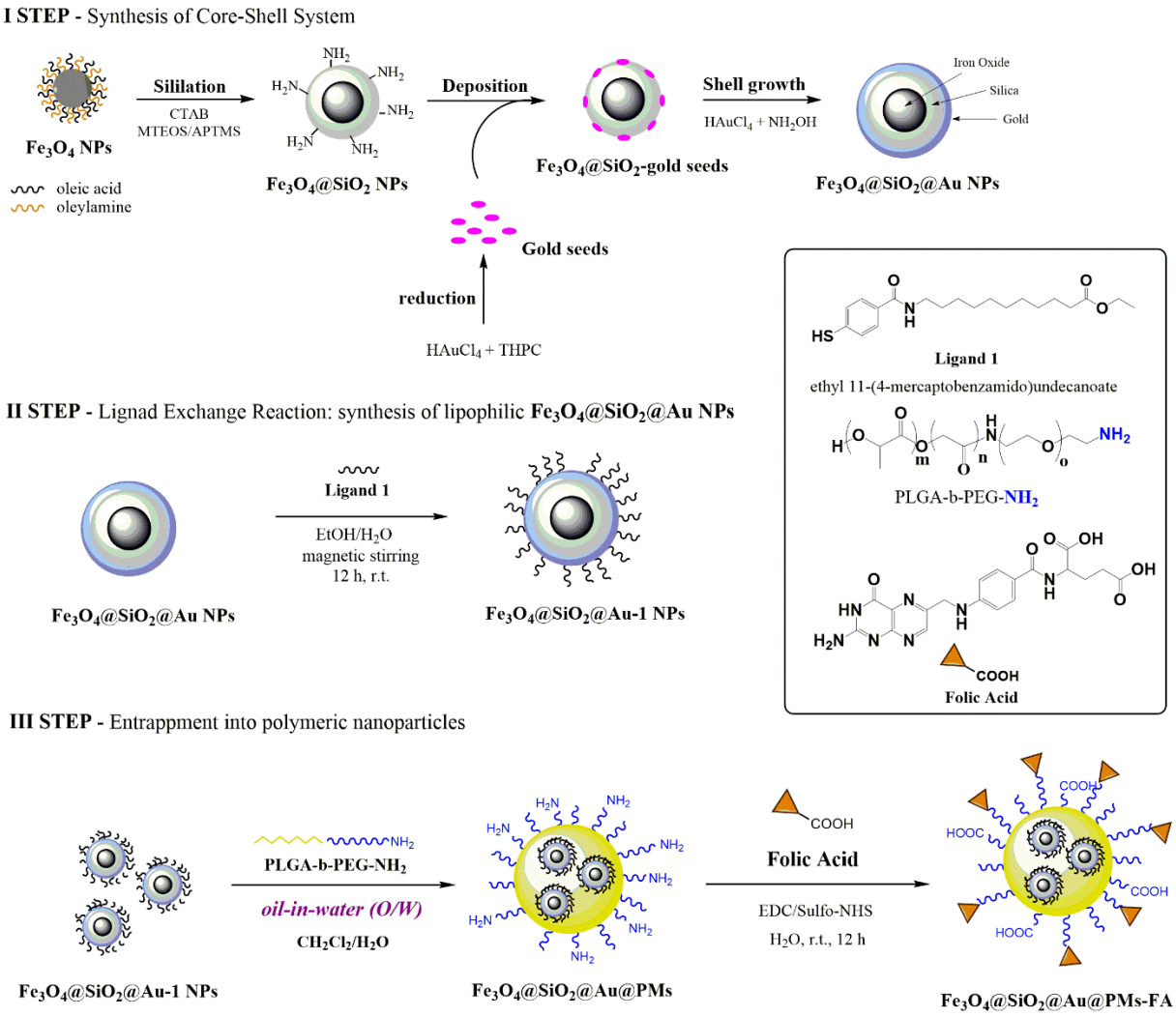

Figure 1: A. Schematic representation of the synthetic process for the obtainment of multilayered Fe_3O_4@SiO_2@Au NPs and their entrappment into polymeric nanomicelles (Fe_3O_4@SiO_2@Au@PNPs)

The different results obtained by DLS and TEM characterizations, can be ascribed to the difference between the hydrodynamic diameter of the Fe_3O_4@SiO_2@Au NPs dissolved in water and their real size, but also to a slight particles aggregation due to the lacking of a steric stabilizer on their surface.

The so-obtained nanoparticles are water-soluble, but lipophilic agents are necessary to achieve the entrapment into the hydrophobic core of polymeric micelles in order to obtain a highly biocompatible final system. In our case, the use of a core-shell system Fe_3O_4@SiO_2@Au NPs allowed to obtain an efficient ligand exchange reaction by taking advantages of the presence of gold on the shell. For this purpose, the ethyl 11-(4-mercaptobenzamido)undecanoate (**1**) was our organic ligand of choice.[17,18] Once modified, the lipophilic NPs was entrapped in the polymeric micelles by using the *oil-in-water* technique.[19] The well-known poly(lactic-*co*-glycolic)-*block*-polyethylene glycol (PLGA-*b*-PEG) was selected due to the Food and Drug Administration (FDA) approval in biomedical formulation and for its ability to form polymeric micelles (PMs) with a lipophilic core that can host lipophilic particles.[25] PLGA-*b*-PEG-NH_2 was used due to the amino functional groups required for the subsequent surface functionalization with folic acid.

The DLS characterization of the Fe_3O_4@SiO_2@Au@PMs particles indicated an hydrodynamic diameter of 157 ± 0.4 nm, a PDI value of 0.3 ± 0.3 and a ζ-potential of -14 mV (Figure S4), while TEM analysis showed the maintenance of

the nanoparticles morphology and their confinement into an organic matrix (Figure 2). In addition, UV-Vis analysis confirmed that the optical proprieties of gold were retained after polymeric entrapment (Figure S7).

In the last preparative step, an active targeting vector has been chemically conjugated on Fe_3O_4@SiO_2@Au@PMs surface.

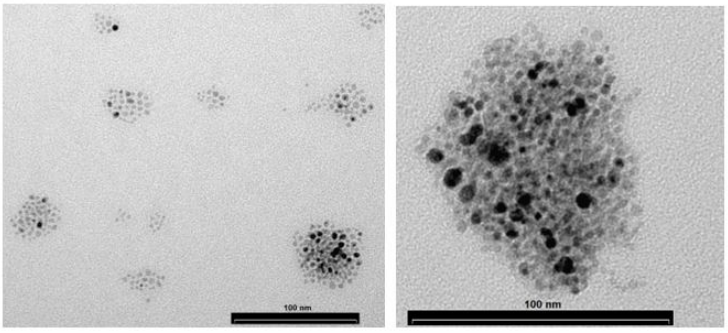

Figure 2: TEM images of Fe_3O_4@SiO_2@Au@PMs. Scale bar 100 nm.

For this purpose, folic acid (FA) was chosen as targeting agent due to its high affinity to the folate receptor, which is a membrane-anchored protein overexpressed on many cancer cells.[20] The conjugation of folic acid was pursued upon EDC activation of its carboxylic group to make it suitable for the reaction with the amine groups at the PMs surface.

The so-obtained Fe_3O_4@SiO_2@Au@PMs-FA were purified and characterized by DLS, AAS, and UV-Vis. DLS analysis showed that the conjugation with FA did not significantly affect the diameter of the particles (165 ± 0.3 nm vs 157 ± 0.4 nm) as well as the polydispersion index that was unchanged. As expected, the ζ-potential of the FA-conjugated particles decreased (from -14 mV to -23 mV) due to the free carboxylate group on the FA molecule. Atomic Absorption Spectroscopy (AAS) indicated that the micelles were characterized by a good concentration of both metals; in particular, iron and gold concentration of 0.1 mM and 1.2 mM were determined, respectively. The developed systems (Fe_3O_4@SiO_2@Au@PMs and Fe_3O_4@SiO_2@Au@PMs-FA) underwent to *in cellulo* and *in vivo* studies in order to evaluate their suitability as MRI and PAI contrast agents.

Cytotoxicity assay

According to the observations available in the literature, it should be noticed that the cytotoxicity outcome of engineered NPs is strongly influenced by testing technique and modalities.

We have used two tumour cell lines as well as a primary normal cell model. The effects of Fe_3O_4@SiO_2@Au@PMs-FA on viability of cells growing as monolayers in culture, was assessed using MTT assay, which has become a standard technique in recent nanoparticle research (Figure 3). Two different FR-positive human carcinoma cells, ovarian (IGROV) and cervical (HeLa) carcinomas, were tested.

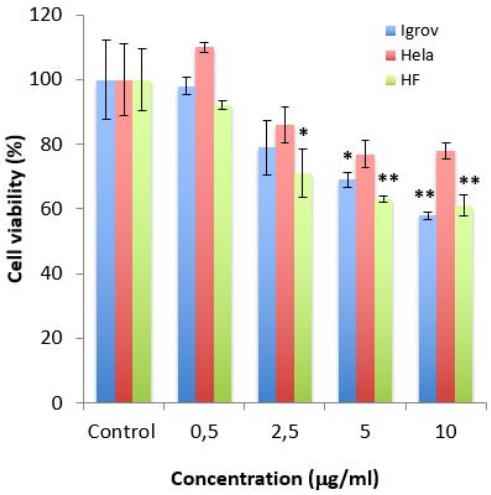

Figure 3. *In vitro* cytotoxicity of nanoparticles at different concentration on IGROV, HeLa and HF cells after incubation for 24 hours. **Note**: Cell viability was evaluated by MTT assay. Results are expressed as means ± SD of experiments performed in triplicate.*p<0.05, **p<0.01 **Abbreviations**: MTT, 3-(4,5-dimethylthiazol-2-yl)-2,5-diphenyltetrazolium bromide; HF, Human Fibroblast.

These cell lines are both known to express high level of FR-α.[21] The Fe_3O_4@SiO_2@Au@PMs-FA did not show any significant cytotoxicity to HeLa cells at different NP concentrations (0.5, 2.5, 5 and 10 µg/ml) for 24 hours. It can be seen that the cell viability still remained as high as 80% at the highest concentration used of 10 µg/ml. These results are in accordance with the previously reported cytotoxicity of magnetic NPs towards HeLa cells.[22,23]

IGROV cells were shown to be more sensitive than HeLa cells and upon increasing NP concentration above 5 µg/ml, a modest statistically significant decrease was noticed in the relative cell viability. Next, primary human fibroblasts (HFs) were chosen as a normal cell model. We can see that HFs were found to be more sensitive to Fe_3O_4@SiO_2@Au@PMs-FA. Our results indicate that after 24 hours of post-treatment HFs showed excellent viability at the concentration of 0.5 µg/ml, but a 40% of decrease in the relative cell survival was observed at the highest concentration of 10 µg/ml.

Comparison of i*n vitro* cytotoxicity of Fe_3O_4@SiO_2@Au@PMs-FA and Fe_3O_4@SiO_2@Au@PMs on IGROV cells after incubation for 24 hours (Figure S5) did not show significant differences between targeted and non-targeted nanoparticles. Overall, MTT assay as a measure of metabolic competence of the cells revealed that: i) in line with previous reports on core-shell NPs, Fe_3O_4@SiO_2@Au@PMs-FA are nontoxic at low dosages but that cell viability decreases at high dosages; ii) fibroblast cells with long doubling times are more susceptible to injury induced by Fe_3O_4@SiO_2@Au@PMs-FA exposure than tumour cells with short doubling times.

Cell fluorescence imaging

As a prelude to *in vivo* studies, we examined cellular uptake of green fluorescently labelled Fe_3O_4@SiO_2@Au@PMs-FA by fluorescence microscopy. Figure 4 shows fluorescence images of IGROV cells after incubation in media containing 10 µg/ml of Fe_3O_4@SiO_2@Au@PMs-FA. For the purpose of distinguishing adsorbed Fe_3O_4@SiO_2@Au@PMs-FA from the internalized one, we used a blue-fluorescent dye (Alexa Fluor® 350) for plasma membrane staining. It can be seen that green fluorescence appears localized inside the cell, suggesting that the cells are effective in taking up Fe_3O_4@SiO_2@Au@PMs-FA.

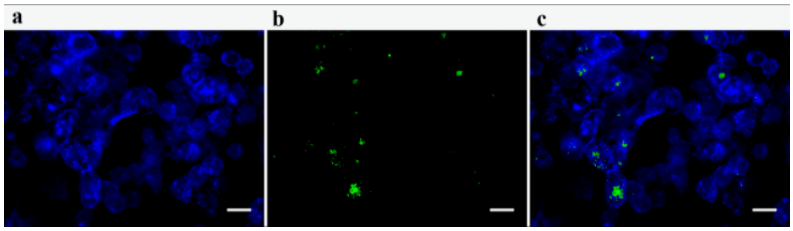

Figure 4. Fluorescence cell imaging. Igrov cells were incubated with nanoparticles (10 mg/ml) at 37°C for 24 hours, to allow nanoparticle cell internalization before microscopy analysis. Representative cell images are shown. DAPI and Alexa Fluor® 350 staining were carried out to visualize nuclei and cell membranes, which appear in blue, while fluorescein-labelled nanoparticles appear in green. (**a**) DAPI and Alexa Fluor® 350 staining; (**b**) Green fluorescence emission; (**c**) Merged images (bar = 20 μm).

MRI studies

Figure 5 shows a series of representative T_{2w} MR images acquired before (pre) and 1, 4, and 24 h after the *i.v.* injection (0.17 mg Fe/kg) of Fe_3O_4@SiO_2@Au@PMs (lower raw) and its folate-targeted form Fe_3O_4@SiO_2@Au@PMs-FA (upper raw) in mice bearing the IGROV subcutaneous xenograft (labelled with "T" in the pre-injection images). The image voxels with a statistically significant T_2-contrast enhancement generated by the Fe_3O_4 core of the particles were highlighted in orange (Figure 5).

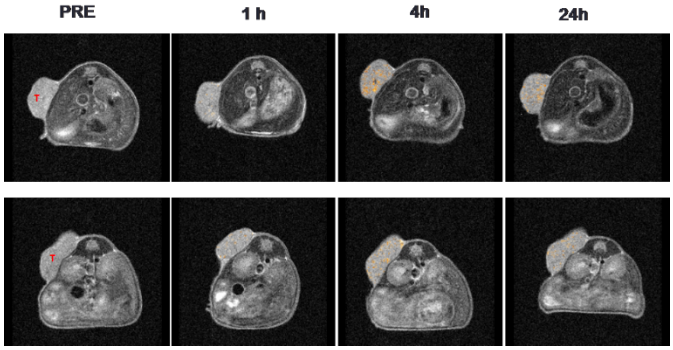

Figure 5: T_{2w} MR images acquired at 1T before, and 1 h, 4 h and 24h after the intravenous injection of Fe_3O_4@SiO_2@Au@PMs-FA (upper panel) or Fe3O4@SiO2@Au@PMs (lower panel) at the dose of 0.17 mg Fe/kg bw. The orange-coloured spots correspond to the pixels with a statistically significant T_2 contrast enhancement.

The result clearly revealed that the NPs-induced tumour contrast is maximum 4 hours post injection for both the nanoparticles, and, importantly, it was higher for the targeted system. In fact, the fraction of contrast-enhanced pixels in the tumour 4 h after the NPs injection was almost three-fold higher for the targeted systems than the control NPs (27.5% vs 10%). Moreover, the data reported in Figure 6 indicate that difference in the MR signal reduction in the tumour region between the two samples is statistically significant ($p<0.05$) only 4 h post injection.

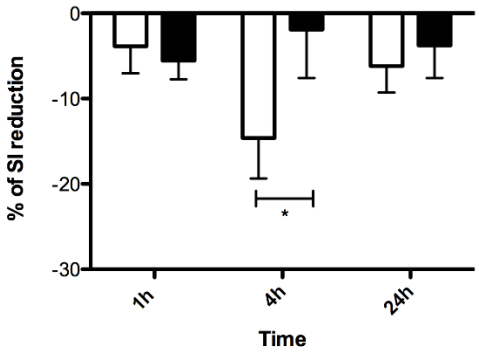

Figure 6: The % Signal Intensity reduction measured in tumor after the i.v. injection of Fe_3O_4@SiO_2@Au@PMs (black) or Fe_3O_4@SiO_2@Au@PMs-FA (white) at different time points. Error bars represent SE of the mean (n=3). (*$p<0.05$)

As expected, a more remarkable T_2 contrast (30-70 % in signal reduction) was measured in the main organs responsible for the blood clearance of nanoparticles, *i.e.* liver and spleen, whereas a negligible contrast was observed in kidneys (Figure S6). The PA spectrum of the particles was characterized by a very broad NIR absorption with a maximum in the range 850-900 nm (Figure S7). Compared to the absorption spectrum of the NPs (shown in Figure S7), the maximum acoustic emission was shifted towards longer wavelength of ca. 120 nm. This observation supports the view that the difference between optical and photoacoustic spectral properties for gold nanoparticles is affected by the size-dependence of the scattering contribution to absportion.[24]

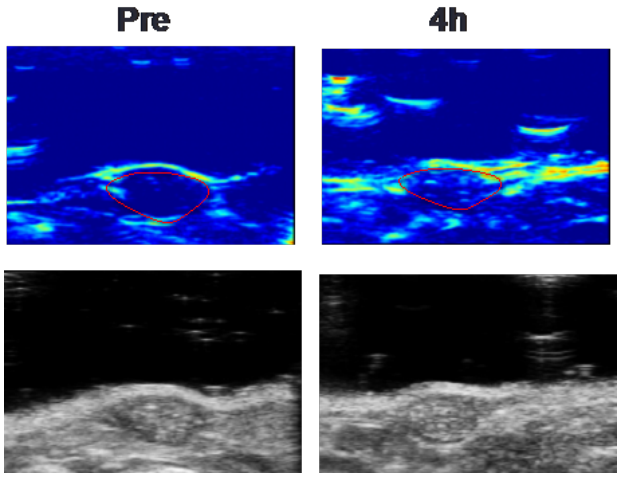

Figure 7: Representative PA (upper) and US (lower) images of the tumour xenograft acquired before (pre) and 4 h after the injection of Fe_3O_4@SiO_2@Au@PMs-FA. PA excitation wavelength was set at 860 nm.

Next, NPs were injected systemically in the tail vein of the tumour bearing mice at a gold concentration of 8.0 mg Au/kg, and PA images of the tumour upon excitation at 860 nm were acquired 4 h post injection, *i.e.* when the particles showed the maximum MRI T_2 contrast. Figure 7 shows a representative example of the results obtained for the targeted system. The position of the xenograft tumour in PAI was determined under US guidance (bottom row images figure 7). The spectral and contrast features of the photoacoustic imaging experiments observed 4 h post injection of the two types of NPs are reported in Figure 8.

In addition to the broad peak arising from the core-shell NPs, the *in vivo* photoacoustic spectra showed the expected sharper signal at ca. 760 nm generated by the absorption of blood haemoglobin. The result obtained strongly confirmed the increased accumulation of the FA-targeted system in the tumour lesion 4 h after their injection.

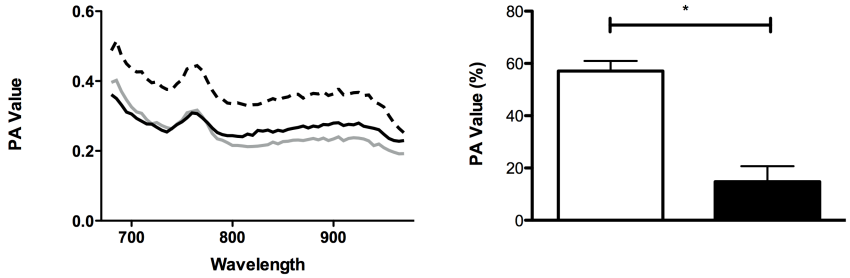

Figure 8: Left: photoacoustic spectra measured in the tumour of animals before (black line) and 4 hours after the injection of Fe_3O_4@SiO_2@Au@PMs-FA (dotted line) or Fe_3O_4@SiO_2@Au@PMs (grey line). Gold injected dose 8 mg/kg. Excitation 860 nm. Right: corresponding PA signal enhancement generated by the targeted system (white) and gold NPs (black). Error bars represent SE of the mean (n=3).

Conclusions

In summary, we have developed the synthesis of iron/silica/gold core-shell nanoparticles and their subsequent surface functionalization and entrapment into polymeric micelles. The advantage of this approach arises from the possibility to manipulate the final dual-imaging nanostructures in water and to build targetable nanostructures. These features have been demonstrated in the case of the ovarian cancer using the Folic Acid targeting agent *in vivo* on tumor-bearing mice showing dual-imaging capabilities, clearly opening promising nanomedicine applications.

Experimental Procedures

Synthesis of native Iron oxide nanoparticles (Fe_3O_4 NPs)

Iron triacetylacetonate (0.002 mmol; 1 eq) was dissolved in diphenyl ether (20 mL). Oleic acid (0.0044 mmol; 2.2 eq), oleyl amine (0.00395 mmol; 2 eq) and hexadecanediol (0.00994 mmol; 5 eq) were then added and the mixture was heated to reflux (267 °C) for 60 min under nitrogen atmosphere, to prevent unwanted oxidation. The mixture was then cooled down to room temperature. The Fe_3O_4 NPs were purified by magnetic precipitation with excess of cold ethanol, dispersed in 5 mL of hexane and washed by four centrifugations (6000 rpm, 45 minutes) in ethanol. The NPs were re-dispersed in 5 mL of hexane (30 mg/mL).

Synthesis of core-shell iron oxide-silica nanoparticles (Fe_3O_4@SiO_2 NPs)

Firstly, hydrosoluble cetyl trimethylammonium bromide (CTAB) micelles loaded with Fe_3O_4 NPs were prepared. 500 mg of CTAB were dissolved in 25 mL of water and sonicated with a tip probe sonicator (600 W, 50% amplitude, 6 min) with 2.5 mL of a solution of Fe_3O_4 NPs (73 mg) in hexane. The hexane was then removed by heating at 70°C for 10 minutes. The as-synthetized micelles were diluted with 125 mL of water and 2.5 mL of ethyl acetate and 3.4 mL of a 28% NH_3 solution were added under vigorous stirring. After 10 minutes, 1.5 mL of methyltriethoxysilane (MTEOS) were added dropwise, and the mixture was stirred 3 days at room temperature (25-30 °C). Then, 1.3 mL of 3-

aminopropyl-methoxysilane (APTMS) were added dropwise and the mixture was stirred 3 other days at room temperature.

The Fe_3O_4@SiO_2 were purified by centrifugation (6000 rpm, 1 h) in water. To remove the CTAB, the Fe_3O_4@SiO_2 NPs were stirred for 30 minutes in a mixture of ethanol/acetic acid 95/5 and centrifuged (6000 rpm, 30 min) for 3 times. Then, the last purifications were performed by centrifugation in ethanol/water 1/1. The Fe_3O_4@SiO_2 NPs were dispersed in 20 mL of ethanol (2 mg/mL).

Synthesis of core-shell iron oxide-silica-gold nanoparticles (Fe_3O_4@SiO_2@Au NPs)

Gold seeds were prepared by reduction of chloroauric acid ($HAuCl_4$) with Tetrakis (Hydroxymethyl)Phosphonium Chloride (THPC). Briefly, 91 mL of water, 3 mL of a 0.2 M NaOH solution, and 2 mL of a THPC solution (120 µL of THPC 80% in 10 mL of water) were mixed. Then, 4 mL of a 25 mM $HAuCl_4$ solution were added under vigorous stirring. Next, 40 mg of Fe_3O_4@SiO_2 NPs were dispersed in 40 mL of ethanol/water 1/1. This mixture was diluted with 100 mL of water and vigorously stirred for 10 minutes. 50 mL of the previous gold seeds solution were added and the mixture was stirred overnight at room temperature. The resulting Fe_3O_4@SiO_2-gold seeds NPs were purified by centrifugation (6000 rpm, 1 h) in water for 4 times, and then dispersed in water (2 mg/mL). The synthesis of an entire shell of gold was performed by a shell growth reaction. $HAuCl_4$ was mildly reduced using hydroxylamine as reducing agent: 101 mg of potassium carbonate were dissolved in 393 mL of water then 7.05 mL of a 25 mM solution of chloroauric acid solution were added. The solution was stirred overnight in darkness at room temperature.

To 100 mL of the so obtained solution, 10 mL of Fe_3O_4@SiO_2-gold seeds NPs solution (20 mg) were added under vigorous stirring. 65 mL of a 1.87 mM hydroxylamine hydrochloride solution were added dropwise in 30 min. The obtained Fe_3O_4@SiO_2@Au NPs were purified by centrifugation (6000 rpm, 30 min) in water, 3 times, and dispersed in water. The size of the gold shell was increased by iteration of this previous shell growth reaction.

Synthesis of lipophilic Fe_3O_4@SiO_2@Au NPs by ligand exchange

The hydrophilic Fe_3O_4@SiO_2@Au NPs were free of any organic coating agent, and they were made lipophilic by organic coating with the ligand ethyl 11-(4-mercaptobenzamido)undecanoate (ligand 1), already synthesized by us.[24] 50 mg of ligand 1 were dissolved in 10 mL of ethanol. 3.5 mg of Fe_3O_4@SiO_2@Au NPs were dispersed in 10 mL of water. The two solutions were mixed, sonicated with ultrasound bath for 45 minutes and let to react overnight on vortex. These lipophilic NPs were purified by centrifugation (6000 rpm, 15 min) in ethanol/water 1/1, 2 times, and dispersed in chloroform.

Synthesis of Fe_3O_4@SiO_2@Au@PMs

A solution of lipophilic Fe_3O_4@SiO_2@Au NPs (3 mg) and PLGA-*b*-PEG-NH_2 (50 mg), obtained by an already reported procedure,[25] in 4 mL of chloroform was prepared. This organic mixture was sonicated (600 W input, 50 % amplitude, 3 min) with 40 mL of water, in an ice bath. The organic solvent was removed under vacuum and the nanoparticles were purified and concentrated to 2 mL with centrifugal filter devices (Amicon Ultra, Ultracel membrane with 100.000 NMWL, Millipore, USA).

***Conjugation of folic acid* (Fe_3O_4@SiO_2@AuNPs@PMs-FA)**

The surface of the PMs was conjugated with the folic acid as a targeting agent. 2 mg of folic acid were dispersed in 0.1 mL drops of DMSO and diluted in 1 mL of water. In order to activate the carboxylic moiety of the active targeting, 1

mL of a 1-ethyl-3-(3-dimethylaminopropyl)carbodiimide (EDC) solution (3.5 mg in 5 mL) and 1 mL of N-hydroxysulfosuccinimide (Sulfo-NHS) solution (4.4 mg in 5 mL) have been added to the acid folic and the obtained solution was stirred for 30 minutes. Then 2 mL of the Fe_3O_4@SiO_2@AuNPs@PMs were added and the mixture was stirred 1 night at room temperature. The conjugated PMs were purified and concentrated into centrifugal filter devices (Amicon Ultra, Ultracel membrane with 100.000 NMWL, Millipore, USA).

***Conjugation of fluorescein* (Fe_3O_4@SiO_2@AuNPs@PMs-FA/fluo) for cellular uptake studies with fluorescence microscopy**

For the synthesis of Fe_3O_4@SiO_2@AuNPs@PMs-FA/fluo, folic acid (2 mg, 4.5 mmol) has been dissolved in DMSO/H_2O (1:10) and activated by adding 1 mL of a 1-ethyl-3-(3-dimethylaminopropyl)carbodiimide (EDC) solution (3.5 mg in 5 mL of H_2O) and 1 mL of N-hydroxysulfosuccinimide (Sulfo-NHS) solution (4.4 mg in 5 mL of H_2O). The obtained solution was stirred for 30 minutes. In a different glass vial, fluorescein isothiocyanate (50 nmol) was dissolved in 1 ml of water. Both folic acid solution and fluorescein solution, were added to 2 mL of the Fe_3O_4@SiO_2@AuNPs@PMs and the mixture was stirred 1 night at room temperature. The conjugated PMs were purified and concentrated into centrifugal filter devices (Amicon Ultra, Ultracel membrane with 100.000 NMWL, Millipore, USA). The Fe_3O_4@SiO_2@AuNPs@PMs-FA/Fluo were characterized by Dynamic Light Scattering (DLS) and showed a hydrodynamic diameter 177.6 ± 9.6 nm, with a PDI of 0.212 ± 0.017 and a ζ-potential of -8.12 mV.

In cellulo experiments

Cells and culture conditions

IGROV and HeLa cell lines (purchased from American Type Culture Collection, ATTC, USA) were cultured in DMEM:F12 (1:1) medium and in DMEM medium respectively, supplemented with 10% fetal bovine serum, 1% L-glutamine and 1% pennicilin/streptomicyn. Primary human fibroblast (HF) culture, obtained from fresh skin biopsy of healthy donor following informed consent (Institute of Maternal and Child Health, IRCSS Burlo Garofolo, Trieste) was cultured in RPMI 1640 medium supplemented with 15% fetal bovine serum, 1% L-glutamine and 1% pennicilin/streptomicyn (all provided by Euroclone, Milano, Italy). Cell cultures were kept at 37°C with humidified atmosphere of 5% CO_2.

Cytotoxicity assay

Cytotoxicity assay was performed using MTT assay (3-(4,5-dimethylthiazol-2-yl)-2,5- diphenyltetrazolium bromide, Sigma Aldrich USA). IGROV, HeLa and HF cells were seeded in 96-well plates (SARSTEDT,
Numbrecht, Germany) at a density of $5x10^3$ cells per well in the culture media described above. Fe_3O_4@SiO_2@Au PMs nanoparticles were suspended in culture media and serially diluted to obtain graduated concentrations. After 24h post seeding, the cells were exposed to different concentrations of Fe_3O_4@SiO_2@Au PMs nanoparticles (0.5, 2.5, 5.0 and 10 µg/ml, respectively). After 24 h post incubation, MTT substrate (Sigma Aldrich, San Luis, MO) was prepared and filtered at 5mg/ml in PBS and added to cells in culture at a final concentration of 0,5 mg/ml. Cell cultures were incubated for 4 h to allow MTT to be metabolized. 100 µl of ethanol were added into each well to re-suspended purple formazan crystal.

The cell viability was measured in absorbance at the wavelength of 570 nm using a plate reading spectrophotometer (Glomax Multi Detection System, Promega Madison WI USA).

Cell fluorescence imaging

IGROV cells were seeded onto 6-well coverglass (Thermo Fischer Scientific Inc, Waltham, MA, USA) at a density of $15x10^4$/well. After one day, the initial medium was replaced by fresh medium containing 10 µg/ml of Fe_3O_4@SiO_2@Au@PMs nanoparticles. 24 hours later, cell cultures were washed twice with phosphate buffered saline (PBS) and incubated with 5µg/ml of Alexa Fluor® 350 (Thermo Fisher Scientific Inc., Waltham, MA, USA) at 37°C for 20 minutes to stain cell membranes. Then, cells were washed twice with PBS, fixed with paraformaldehyde (PFA) 4% for 30 minutes and slides were mounted using Vectashield mounting medium for fluorescence with DAPI to stain cellular nuclei (Vector laboratories Inc. Burlingame, CA). Finally, cells were observed by fluorescence microscopy: fluorescent images were acquired by using an inverted microscope with a CCD camera and the objectives lens 40X. (Axioplan2, with Axiocam MRc, ZEISS Oberkochen Germany)

Statistical analysis

Statistical verification of the differences of cell viability between treated and control cells for each experiment and concentration was done using an unpaired Welch Two sample t-test. A p-value of less than 0.05 was considered significant.

In vivo experiments

Tumor animal model

Balb/C nude mice (nu/nu, aged 6 weeks and weighed 18-22 g) were purchased from Harlan Laboratories. Ten million of IGROV-1 cells were suspended in 1:1 Matrigel™: RPMI-1640 medium and subcutaneously injected in the back of the animal. Tumor growth was monitored after inoculation by palpation and caliper measurement. When the tumor reached 0.4-0.6 cm in diameter, the animals were enrolled in the *in vivo* imaging studies. Each experimental group consisted of 3 animals. All the experiments involving animals were performed according to the authorization (229/2016-PR) obtained by the National Ministry of Health.

MRI and PAI experiments

MRI experiments were performed at a magnetic field strength of 1 T on Bruker ICON (Bruker, Germany). T_{2w} images were obtained using the multiecho RARE sequence (relevant acquisition parameters: TR 2000 ms, TE 50 ms, FA 180°, NEX 4, MTX=192 x 192, FOV 3.5 cm).

MR images were analysed to calculate the relative signal intensity (rSI) in liver, spleen, kidneys, and tumour according to the following equation:

$$rSI_{(organ)} = (SI_{(organ)} - SI_{(muscle)})/(SI_{(organ)} + SI_{(muscle)})$$

where $SI_{(organ)}$ is the mean of three ROIs drawn on the organ, and $SI_{(muscle)}$ is the corresponding value measured on the paraspinal muscle. Then, the % of the Signal Intensity Reduction was calculated comparing the $rSI_{(organ)}$ before and after the injection of the agent.

Photoacoustic images were acquired on VEVO-2100 LAZR (VisualSonics - Fujifilm System) using the LZ250 transducer (broadband frequency 13-24 MHz) in spectrum modality (wavelength values ranging from 680 to 960 nm, 1

nm step size, pulse of 4-6 ns, transducer gain 38 dB, The spot size was 1x24mm with a full field of view width of 14-23 mm. The acquisition rate was 5 frames per second.

The PA signal intensity was calculated using the VEVO lab tool. All values were normalized in function of the number of pixels of each ROI. The particles (Fe_3O_4@SiO_2@Au@PMs or Fe_3O_4@SiO_2@Au@PMs-FA) were injected intravenously in single bolus at a dose of 0.17 mg Fe/kg bw. MRI and PAI acquisitions were performed at times 0 (pre contrast), 1, 4, and 24 hours post injection. Animals were anaesthetized with isofluorane gas (2%) in 98% O_2. During MRI experiments, anaesthesia was maintained by adjustment of gas level in function of the breath rate. Animals were maintained warmed at 37°C during all acquisitions.

Associated content

*S Supporting Information

The Supporting Information is available free of charge on the ACS Publications website at DOI:

Figures showing DLS spectra, TEM images, EDX analysis, UV-Visible Absorption photoacoustic spectra.

Author Information

Corresponding Authors: Mauro Comes Franchini

*E-mail: mauro.comesfranchini@unibo.it

Present AddressesDepartment of Industrial Chemistry "Toso Montanari", Viale Risorgimento 4, 40136, Bologna, Italy.

[1]Sousa F., Sanavio B., Saccani A., Tang Y., Zucca I, Carney T.M., Mastropietro A., Jacob Silva PH. , Carney R.P., Schenk K. et al., (2017*)* Superparamagnetic Nanoparticles as High Efficiency Magnetic Resonance Imaging T_2 Contrast Agent, *Bioconjugate Chem*., *28*, 161-170

[2]Siti J. .M., Moses A. S., MacKay J. A..(2010) Imaging and drug delivery using theranostic nanoparticles. *Advanced drug delivery reviews, 62*, 1052-1063.

[3] Stjerndahl M., Andersson M., Hall H.E., Pajerowski D.M., Meisel M.W., Duran R.S.. (2008) Superparamagnetic Fe_3O_4/SiO_2 Nanocomposites: Enabling the Tuning of Both the Iron Oxide Load and the Size of the Nanoparticles. *Langmuir*, *24(7)*, 3532-3536.

[4] Brinker C.J., Scherer G.W.. (2013) Sol-Gel Science 1th Edition, The Physics and Chemistry of Sol-Gel Processing, pp 838-880, *Academic press.*

[5]Kim J., Park S., Lee J.E., Jin S.M., Lee J.H., Lee I.S., Yang I., Kim J.-S., Kim S.K, Cho M.-H.,et al. (2006) Designed Fabrication of Multifunctional Magnetic Gold Nanoshells and Their Application to Magnetic Resonance Imaging and Photothermal Therapy *Angew. Chem. Int. Ed*., *45*, 7754-7758.

[6]Ji X., Shao R., Elliott A.M., Stafford R.J., Esparza-Coss E., Bankson J.A., Liang G., Luo Z.-P., Park K., Markert J.T. at al. (2007) Bifunctional Gold Nanoshells with a Superparamagnetic Iron Oxide-Silica Core Suitable for Both MR Imaging and Photothermal Therapy**,** *J. Phys. Chem. C. Nanomater. Interfaces, 111(17),* 6245-6251.

[7] Melancon M.P., Elliott A., Ji X., Shetty A., Yang Z., Tian M., Taylor B., Stafford R.J., Li C..(2011) Theranostics with multifunctional magnetic gold nanoshells: photothermal therapy and t_2* magnetic resonance imaging. *Invest Radiol*., ***46(2),*** 132-140.

[8] Lee D.E., Koo H., Sun I.C., Ryu J.H., Kim K., Kwon I.C..(2012) Multifunctional nanoparticles for multimodal imaging and theragnosis *Chem. Soc. Rev.*, *41(7),* 2656-2672.

[9]Yue L., Wang J., Dai Z.,Hu Z., Chen X., Qi Y., Zheng X.,Yu D..(2017), pH-Responsive, Self-Sacrificial Nanotheranostic Agent for Potential In Vivo and In Vitro Dual Modal MRI/CT Imaging, Real-Time, and In Situ Monitoring of Cancer Therapy **,** *Bioconjugate Chem,* DOI***:****10.1021/acs.bioconjchem.6b00562*

[10] Niederhauser J.J., Jaeger M., Lemor R., Weber P., Frenz M.. (2005) Combined ultrasound and optoacoustic system for real-time high-contrast vascular imaging *in vivo. IEEE Trans. Med. Imaging*, 24(4), 436-440.

[11] Mallidi S., Luke G.P., Emelianov S.. (2011) Photoacoustic imaging in cancer detection, diagnosis, and treatment guidance *Trends Biotechnol.,* 29(5) 213-221.

[12] Zhou M., Singhana B., Liu Y., Mitcham T., Wallace M.J., Stafford R.J., Bouchard R.R., Melancon M.P.. (2015) Photoacoustic- and Magnetic Resonance-Guided Photothermal Therapy and Tumor Vasculature Visualization Using Theranostic Magnetic Gold Nanoshells. *J. Biomed. Nanotechnol*., 11(8), 1442-1450.

[13] Marchetti C, Palaia I, Giorgini M, De Medici C, Iadarola R, Vertechy L, Domenici L, Di Donato V, Tomao F, Muzii L, et al. (2014) Targeted drug delivery via folate receptors in recurrent ovarian cancer: a review. *Onco Targets Ther*., *7*, 1223-36.

[14] Sun S., Zeng H., (2002), Size-Controlled Synthesis of Magnetite Nanoparticles**,** *J. Am. Chem. Soc.*, 124(28), 8204-8205.

[15] Stöber W., Fink A., Bohn E., (1968) Controlled Growth of Monodisperse Silica Spheres in the Micron Size Range *J. Colloid Interface Science*, 26, 62-69.
[16] Duff D.G., Baiker A., Edwards P.P, (1993), A new hydrosol of gold clusters, *Chem. Commun*., *1*, 96-98.
[17] Locatelli E., Broggi F., Ponti J., Marmorato P., Franchini F., Lena S., Comes Franchini M.. (2012) Lipophilic Silver Nanoparticles and Their Polymeric Entrapment into Targeted-PEG-Based Micelles for the Treatment of Glioblastoma. *Adv. Healthcare Mater.,1*, 342-347.
[18] Locatelli E., Monaco I., Comes Franchini M., (2015) Surface modifications of gold nanorods for applications in nanomedicine *RSC Adv*., *5*, 21681-21699.
[19] Reis C.P., Neufeld R.J., Ribeiro A.J., Veiga F.. (2006) Nanoencapsulation I. Methods for preparation of drug-loaded polymeric nanoparticles. *Nanomedicine: Nanotechnology, Biology and Medicine*. 2(1), 8-21.
[20] Fan N.-C., Cheng F.-Y., Ho J.A., Yeh C.-S.. (2012) Photocontrolled Targeted Drug Delivery: Photocaged Biologically Active Folic Acid as a Light-Responsive Tumor-Targeting Molecule. *Angew. Chem. Int. Ed.*, *51*, 8806-8810.
[21] Kelley K. M., Rowan B. G., Ratman M., (2003) Modulation of the folate receptor alpha gene by the estrogen receptor: mechanism and implications in tumor targeting. *Cancer Res*., 63(11), 2820-2828.
[22] Lidi C., Chen X., Yanan X., Xiaoyang X..(2015) A redox stimuli-responsive superparamagnetic nanogel with chemically anchored DOX for enhanced anticancer efficacy and low systemic adverse effects . *J. Mater. Chem. B*, *3*, 8949-8962.
[23]Zheng D.W., Lei Q., Si Chen, Qiu W.X., Liu M.Y., Chen X., Ding Y.X., Li P.H., Zhang Q.Y., Xu Z.S, et al..(2015) Supermolecular theranostic capsules for pH-sensitive magnetic resonance imaging and multi-responsive drug delivery. *J. Mater. Chem. B*, *3*, 8499-8507.
[24]Feis A., Gellini C., Salvi P.R., Becucci M., (2014) Photoacoustic excitation profiles of gold nanoparticles**.** Photoacoustics, *2*, 47-53.
[24] Gentili D., Ori G., Comes Franchini M. (2009) Double phase transfer of gold nanorods for surface functionalization and entrapment into PEG-based nanocarriers. *Chem. Commun*., *39*, 5874-5876.
[25] Locatelli E., Comes Franchini M. (2012). Biodegradable PLGA-b-PEG polymeric nanoparticles: synthesis, properties, and nanomedical applications as drug delivery system. *J. Nanopart. Res.*, 14, 1316.